Towards high-resolution ptychographic x-ray diffraction microscopy

Yukio Takahashi,[1,*] Akihiro Suzuki,[1] Nobuyuki Zettsu,[2] Yoshiki Kohmura,[3] Yasunori Senba,[4] Haruhiko Ohashi,[4] Kazuto Yamauchi,[1] and Tetsuya Ishikawa[3]

[1]*Graduate School of Engineering, Osaka University, 2-1 Yamada oka, Suita, Osaka 565-0871, Japan*

[2]*Department of Materials, Physics and Energy Engineering, Graduate School of Engineering, Nagoya University, Furocho, Chikusa-ku, Nagoya 4648603, Japan*

[3]*RIKEN SPring-8 Center, 1-1-1 Kouto, Sayo-cho, Sayo, Hyogo 679-5148, Japan*

[4]*Japan Synchrotron Radiation Research Institute, SPring-8, 1-1-1 Kouto, Sayo-cho, Sayo, Hyogo 679-5198, Japan*

(Received 11 March 2011; published 13 June 2011)

Ptychographic x-ray diffraction microscopy is a lensless imaging technique with a large field of view and high spatial resolution, which is also useful for characterizing the wavefront of an x-ray probe. The performance of this technique is degraded by positioning errors due to the drift between the sample and illumination optics. We propose an experimental approach for correcting the positioning errors and demonstrate success by two-dimensionally reconstructing both the wavefront of the focused x-ray beam and the complex transmissivity of the weakly scattering objects at the pixel resolution of better than 10 nm in the field of view larger than 5 μm. This method is applicable to not only the observation of organelles inside cells or nano-mesoscale structures buried within bulk materials but also the characterization of probe for single-shot imaging with x-ray free electron lasers.

DOI: 10.1103/PhysRevB.83.214109 PACS number(s): 42.30.−d, 07.85.−m, 41.50.+h, 61.46.−w

I. INTRODUCTION

X-ray diffraction microscopy[1] (XDM) is a lensless x-ray imaging technique based on coherent diffraction measurements and iterative phasing methods. After the first demonstration in transmission geometry[2] and reflection geometry,[3] applications to various materials[4,5] and biological systems[6–8] have emerged in synchrotron experiments. Very recently, a single mimivirus has been observed by XDM using the single-pulse beam of an x-ray free electron laser (XFEL).[9] The original geometry of XDM, in which the sample is illuminated with an x-ray plane wave, is limited to an isolated object. Two experimental approaches were proposed to remove this important limitation. One is keyhole imaging,[10] in which a finite expanding beam can be used to define a finite extent for the wavefield leaving the object. The other approach is the scanning scheme,[11] which is called "ptychography," in which a probe is scanned across the sample and the diffraction pattern is observed at each beam position.

Ptychographic x-ray diffraction microscopy (PXDM) was first demonstrated in 2007.[12] In PXDM, coherent diffraction patterns are collected so that the illumination area overlaps with the neighboring position. The complex transmission function of objects is iteratively retrieved using a ptychographical iterative engine,[13] which is an iterative phasing method. Recently, PXDM has been applied to the large-field-of-view and high-resolution imaging of biological samples in two[14,15] and three[16] dimensions. PXDM enables us also to reconstruct the wavefront of probes by using modified algorithms,[16,17] which has been applied to the characterization of the complex wavefield of x-ray nanobeams.[19–21] The spatial resolution of PXDM is limited, in principle, only by the x-ray wavelength and the largest scattering angle recorded. The use of highly focused incident x-ray beams is effective for collecting high angle diffraction data at a high signal-to-noise ratio.[22–24] Note that PXDM is very sensitive to drift between the sample and illumination optics,[21] indicating that both the resolution and field of view are degraded by positioning errors of the x-ray probe. Therefore, exact and reliable control of the x-ray probe is crucial for the high-resolution imaging in PXDM. Thus, experimental and/or computational[25] approaches for correcting the positioning errors are highly required.

In this paper, we describe an experimental approach toward high-resolution PXDM. We propose a method of correcting the positioning errors using reference points. We demonstrate success by quantitatively observing weakly scattering objects in a large area and visualizing the detailed structures of the wavefront of the focused x-ray beam. We discuss the possibility of applications using next-generation x-ray sources.

II. EXPERIMENTAL DETAILS

The experiment of PXDM with datum reference was carried out at BL29XUL (Ref. 26) in SPring-8. Figure 1(a) shows a schematic of the experimental setup. The x-ray beam was two-dimensionally focused using Kirkpatrick-Baez (KB) mirrors at the x-ray energy of 11.8 keV.[24] The flux of the focused x rays was estimated to be $\sim 3\times 10^7$ photons/s. Samples were located at the focal plane. Figures 1(b) and 1(c) show the scanning electron microscopy (SEM) image of a test object and nanoparticles on the SiN membrane as the samples. The test object is a Siemens star pattern, which consists of a 200-nm-thick nanostructured tantalum layer on a SiC membrane and contains the finest lines and spaces of 50 nm. The nanoparticles are gold of $\sim$200 nm size fabricated by shape-controlled synthesis,[27] which was supported by a SiN membrane. The test object and gold nanoparticle sample were illuminated in 7×7 and 5×7 overlapping fields of view, respectively, that were spaced by 500 nm. The sample position was precisely controlled by using piezo stages with capacitives sensors. X-ray exposure times of the in-vacuum front-illuminated charge-coupled device (CCD) detector at each position were 90 s for the test object and 190 s for the nanoparticles. Both the sample chamber and focusing system were set up in a constant-temperature room. The temperature change was less than 0.05 K during the

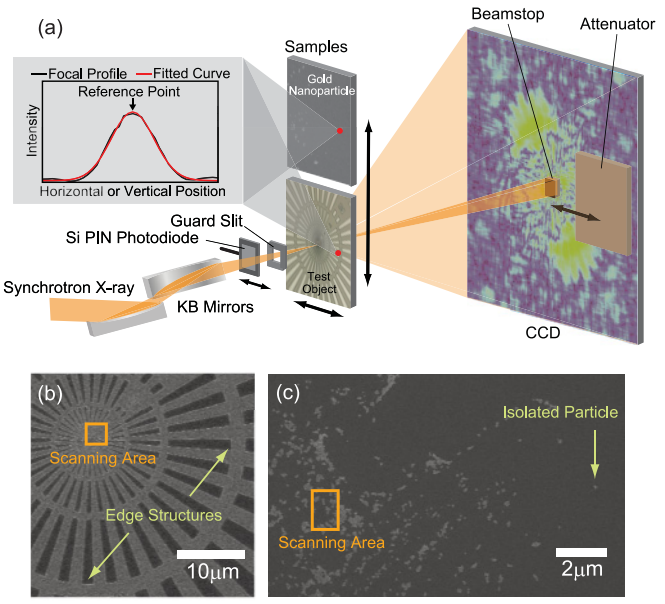

FIG. 1. (Color online) (a) Schematic of high-resolution ptychographic hard x-ray diffraction microscope. SEM image of (b) test object and (c) gold nanoparticles of the samples. The x rays of 11.8 keV were two-dimensionally focused using KB mirrors. Samples were located at the focal plane. To reduce parasitic scattering x rays from the mirrors, guard slits were placed between the mirrors and the focus. Forward-diffracted x-ray photons at each position were detected using the CCD detector with a pixel size of 20 × 20 μm^2 placed 2024 mm downstream of the sample. A direct beam stop or aluminum attenuator was placed in front of the CCD detector. X-ray flux was measured using a Si-PIN-photodiode after taking the diffraction pattern at each position.

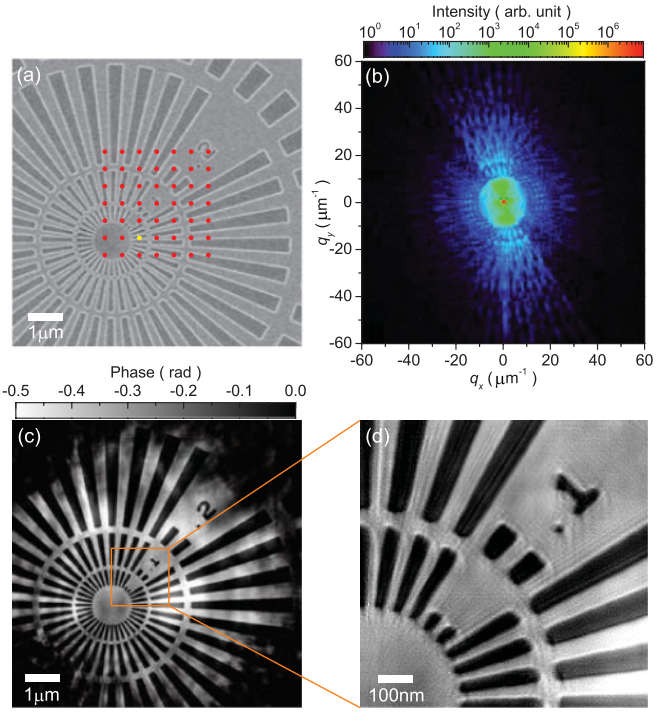

FIG. 2. (Color online) (a) SEM image of the test object. Round dots indicate the x-ray irradiated positions. (b) Coherent diffraction pattern of the test object observed at the position indicated by a light-colored dot in (a). The diffraction pattern is composed of an array of 1277 × 1277 pixels. q is defined as $|q| = 2\sin(\Theta/2)/\lambda$, where Θ is the scattering angle and λ is the x-ray wavelength. (c) Reconstructed phase map of the test object. The pixel size is 8.3 nm. The total pixel size is 1000 × 1000. (d) Enlarged phase map of the area indicated by a square in (c).

measurement of each sample. In the scanning measurement, edge structures [see Fig. 1(b)] in the test object and an isolated particle [see Fig. 1(c)] were used as the reference point. Before measuring the diffraction pattern at each position, the dark-field knife-edge scan method[28] was performed at the edge structure or the isolated particle to precisely measure the drift of the focused beam position using the CCD detector. The intensity profiles were fitted using a Gaussian function, and then the peak position of the fitting curve was defined as the reference point. The positioning error was corrected on the basis of the datum reference. Ptychograpic diffraction pattern data were separately collected to cover a wide-q range, i.e., a part of the direct beam, low-q diffraction, and high-q diffraction, by switching the beamstop and the 2-mm-thick aluminum attenuator. The diffraction patterns were patched and then those intensities were normalized by the flux value. The total measurement time including read-out time from the CCD, beamstop motion, flux data collection, and positioning error correction was ∼10 h for each sample. The time spent for the positioning error correction was ∼20% of the total measurement time.

III. RESULTS AND DISCUSSION

A. Image reconstruction of a test object

Figure 2(a) shows the SEM image of the test object. Round dots indicate the x-ray irradiation positions. Figure 2(b) shows the coherent diffraction pattern at the position indicated by a light-colored dot in Fig. 2(a), where the low-q and high-q diffraction patterns were stitched on the basis of diffraction intensities. The diffraction pattern shows high contrast in the wide-q range and a resolution of 8.3 nm at the edge. Next, both the complex transmission function of the object and the complex illuminating wave field were reconstructed from the 49 diffraction patterns using the extended ptychographical iterative engine[18] within the weak phase object approximation.[15] The reconstruction was started from an initial Gaussian wave field and a flat object of unit transmission. The iterative process was continued for up to 1×10^4 iterations. Figure 2(c) shows the reconstructed phase of the complex transmission function of the object with a pixel size of 8.3 nm. The field of view is ∼10 × 10 μm^2, which is considerably larger than the scanning area of 3 × 3 μm^2. The phase shift is ∼0.2 rad, which is almost equal to the theoretical value of 0.22 rad. The enlarged image [Fig. 2(d)] sharply resolves the 50 nm lines and spaces. The artifacts due to positioning errors cannot be seen, which indicates that the correction of positioning errors worked well.

B. Reconstruction of the wave field of the x-ray probe

Figure 3(a) shows the intensity and phase maps of the reconstructed wave field of the probe. The intensity and phase

distributions are similar to those of Fraunhofer diffraction from a rectangular aperture, which implies that the x-ray beam was ideally focused in the present experiment. Figure 3(b) shows the cross-sectional plots through the peak top of the intensity map and beam profiles by the dark-field knife-edge scan method for comparison. A good agreement of both profiles indicates high reliability of the present ptychographic probe reconstruction, being understood also by the fact that the sample image was reconstructed in the field of view larger than the scanning area [see Fig. 2(c)]. The full width at half maximum (FWHM) of the central peak was approximately 570(h) × 610(v) nm^2, which is close to 500(h) × 511(v) nm^2 of the diffraction-limited focal spot size. The six-order diffraction spot is clearly visible, which is ∼4 μm away from the main peak and has an intensity of ∼1/1000 of the main peak. This is the first two-dimensional visualization of the wavefront of a nearly diffraction-limited x-ray nanobeam produced by KB mirror optics.

C. High-resolution observation of gold nanoparticles

Next, the phase image of the gold nanoparticles was reconstructed. Here, the complex wavefield shown in Fig. 3(a) was used as the illumination function. The iterative process was continued for up to 1 × 10^3 iterations. Figures 4(a) and 4(b) show the reconstructed phase and SEM image in the same region after the x-ray radiation, respectively. The features of the particles seen in both images are in good

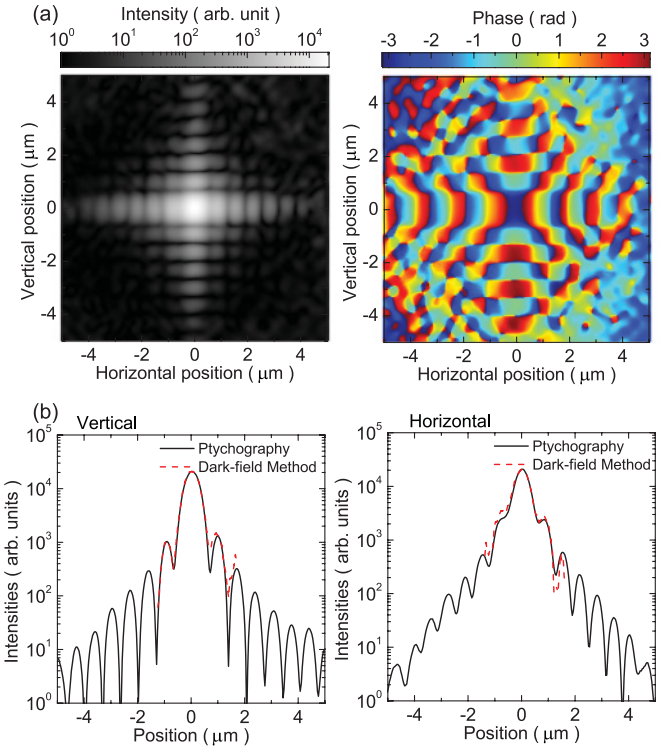

FIG. 3. (Color online) (a) Intensity and phase of the reconstructed wave field at the focal plane of the focused x-ray beam. (b) (Solid line) Cross sections through the peak of the reconstructed intensity. (Dotted line) Focal profiles measured by the dark-field knife-edge scan method using the edge structures of the test object.

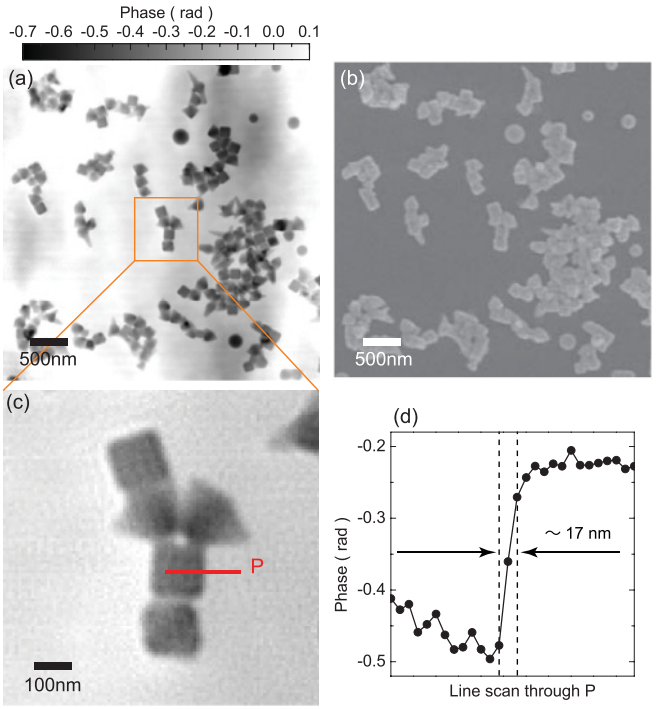

FIG. 4. (Color online) (a) Reconstructed phase map of the gold nanoparticles. The pixel size is 8.3 nm. The total pixel size is 200 × 200, which is a part of the reconstructed phase image. (b) SEM image of the gold nanoparticles in the same area as (a). (c) Enlarged phase image of the area indicated by a square in (a). (d) Cross-sectional plot through line P in (c).

agreement. The phase image can be a projection of the electron density distribution of the object, while the SEM image shows the contrast of the surface structure. The difference in thickness can be confirmed clearly as a contrast in both images. Figure 4(c) shows the enlarged image of the phase. The nanocube particles are clearly seen in Fig. 4(c). Figure 4(d) shows a cross-sectional plot of the nanocube through line P indicated in Fig. 4(c). The edge structure is considerably sharp and its width is ∼17 nm which is the best resolution achieved by PXDM. The phase shift of the edge is ∼0.2 rad, which roughly corresponds to the value estimated from the edge length of the gold nanocube.

IV. CONCLUSION

We have established high-resolution PXDM through the illumination of a highly focused hard x-ray beam at the exact position on the samples. The present method can be applied to not only the observation of organelles inside cells or nano-mesoscale structures buried within metallic materials of more than 10 μm size but also the high-accuracy characterization of the wavefield of the x-ray nanobeams. To shorten the measurement time and improve the spatial resolution, an increase in coherent x-ray intensities is required. The next-generation light source such as upgraded synchrotrons and energy recovery linac will meet this demand. Note that, as the resolution approaches the wavelength, the thickness effect of

objects plays a significant role in XDM.[29,30] The propagation of the diffracted x rays inside the object must be considered, and hence, theoretical progress is crucially necessary.

Keyhole XDM is also a promising approach for large-field-of-view and high-resolution x-ray imaging, which can be improved as a single-shot imaging technique by using XFELs. In keyhole XDM, the illumination function must be defined beforehand. For example, the wavefield at focus of the Fresnel zone plate (FZP) was retrieved by using the intensity far from the focal plane and the basic knowledge on the geometry of FZP optic.[31] The present setup can be changed to the setup of the keyhole imaging by moving the sample to the defocus position. Therefore, both the probe reconstruction and low-resolution observation are performed by PXDM under XFEL radiation with attenuation. Then, single-shot high-resolution imaging at the selected field of view is carried out by keyhole XDM using an XFEL single pulse without attenuation. The combination procedure using mirror optics might be highly useful for imaging studies using XFELs. We believe that this approach will open up the frontier of the large-field-of-view (>10 μm), high-resolution (<10 nm), and high-speed imaging (<50 fs).

ACKNOWLEDGMENTS

This research has been carried out in the Program of Promotion of Environmental Improvement to Enhance Young Researcher's Independence, the Special Coordination Funds for Promoting Science and Technology from the Ministry of Education, Culture, Sports, Science and Technology (MEXT). This work was also partly supported by funds from a Grant-in-Aid for Young Scientists (Grant No. 21686060), Challenging Exploratory Research (Grant No. 22651040), Scientific Research on Priority Areas (Grant No. 23102504), the Global COE Program "Center of Excellence for Atomically Controlled Fabrication Technology," Core Research for Evolutional Science and Technology from MEXT. The authors would like to acknowledge JTEC Corporation for fabrication of the mirrors and H. Kishimoto for the construction of the temperature stabilization system.

*takahashi@prec.eng.osaka-u.ac.jp

[1] H. N. Chapman and K. A. Nugent, Nat. Photonics **30**, 833 (2010).
[2] J. Miao, P. Charalambous, J. Kirz, and D. Sayre, Nature (London) **400**, 342 (1999).
[3] I. K. Robinson, I. A. Vartanyants, G. J. Williams, M. A. Pfeifer, and J. A. Pitney, Phys. Rev. Lett. **87**, 195505 (2001).
[4] M. C. Newton, S. J. Leake, R. Harder, and I. K. Robinson, Nature Mater. **9**, 120 (2010).
[5] Y. Takahashi, N. Zettsu, Y. Nishino, R. Tsutsumi, E. Matsubara, T. Ishikawa, and K. Yamauchi, Nano Lett. **10**, 1922 (2010).
[6] Y. Nishino, Y. Takahashi, N. Imamoto, T. Ishikawa, and K. Maeshima, Phys. Rev. Lett. **102**, 018101 (2009).
[7] J. Nelson, X. Huang, J. Steinbrener, D. Shapiro, J. Kirz, S. Marchesini, A. M. Neiman, J. J. Turner, and C. Jacobsen, Proc. Natl. Acad. Sci. USA. **107**, 7235 (2010).
[8] H. Jiang, C. Song, C. C. Chen, R. Xu, K. S. Raines, B. P. Fahimian, C. H. Lu, T. K. Lee, A. Nakashima, J. Urano, T. Ishikawa, F. Tamanoi, and J. Miao, Proc. Natl. Acad. Sci. USA. **107**, 11234 (2010).
[9] M. M. Seibert, T. Ekeberg, F. R. N. C. Maia, M. Svenda, J. Andreasson, O. Jönsson, D. Odić, B. Iwan, A. Rocker, D. Westphal *et al.*, Nature (London) **470**, 78 (2011).
[10] B. Abbey, K. A. Nugent, G. J. Williams, J. N. Clark, A. G. Peele, M. A. Pfeifer, M. D. deJonge, and I. McNulty, Nat. Phys. **4**, 394 (2008).
[11] J. M. Rodenburg and R. H. T. Bates, Philos. Trans. R. Soc. London, Ser. A **339**, 521 (1992).
[12] J. M. Rodenburg, A. C. Hurst, A. G. Cullis, B. R. Dobson, F. Pfeiffer, O. Bunk, C. David, K. Jefimovs, and I. Johnson, Phys. Rev. Lett. **98**, 034801 (2007).
[13] H. M. L. Faulkner and J. M. Rodenburg, Phys. Rev. Lett. **93**, 023903 (2004).
[14] K. Giewekemeyer, P. Thibault, S. Kalbfleisch, A. Beerlink, C. M. Kewish, M. Dierolf, F. Pfeiffer, and T. Salditt, Proc. Natl. Acad. Sci. USA. **107**, 529 (2009).
[15] M. Dierolf, P. Thibault, A. Menzel, C. M. Kewish, K. Jefimovs, I. Schlichting, K. König, O. Bunk, and F. Pfeiffer, New J. Phys. **12**, 035017 (2010).
[16] M. Dierolf, A. Menzel, P. Thibault, P. Schneider, C. M. Kewish, R. Wepf, O. Bunk, and F. Pfeiffer, Nature (London) **467**, 436 (2010).
[17] P. Thibault, M. Dierolf, O. Bunk, A. Menzel, and F. Pfeiffer, Ultramicroscopy **109**, 338 (2009).
[18] A. M. Maiden and J. M. Rodenburg, Ultramicroscopy **109**, 1256 (2009).
[19] P. Thibault, M. Dierolf, A. Menzel, O. Bunk, C. David, and F. Pfeiffer, Science **321**, 321 (2008).
[20] C. M. Kewish, P. Thibault, M. Dierolf, O. Bunk, A. Menzel, J. Vila Comamala, K. Jefimovs, and F. Pfeiffer, Ultramicroscopy **110**, 325 (2010).
[21] A. Schropp, P. Boye, J. M. Feldkamp, R. Hoppe, J. Patommel, D. Samberg, S. Stephan, K. Giewekemeyer, R. N. Wilke, T. Salditt, J. Gulden, A. P. Mancuso, I. A. Vartanyants, E. Weckert, S. Schöder, M. Burghammer, and C. G. Schroer, Appl. Phys. Lett. **96**, 091102 (2010).
[22] I. K. Robinson, F. Pfeiffer, I. Vartanyants, Y. Sun, and Y. Xia, Opt. Express **11**, 2329 (2003).
[23] C. G. Schroer, P. Boye, J. M. Feldkamp, J. Patommel, A. Schropp, A. Schwab, S. Stephan, M. Burghammer, S. Schoder, and C. Riekel, Phys. Rev. Lett. **101**, 090801 (2008).
[24] Y. Takahashi, Y. Nishino, R. Tsutsumi, H. Kubo, H. Furukawa, H. Mimura, S. Matsuyama, N. Zettsu, E. Matsubara, T. Ishikawa, and K. Yamauchi, Phys. Rev. B **80**, 054103 (2009).
[25] M. Guizar-Sicairos and J. R. Fienup, Opt. Express **16**, 7264 (2008).
[26] K. Tamasaku, Y. Tanaka, M. Yabashi, H. Yamazaki, N. Kawamura, M. Suzuki, and T. Ishikawa, Nucl. Instrum. Methods Phys. Res. A **467–468**, 686 (2001).
[27] T. K. Saum and C. J. Murphy, J. Am. Chem. Soc. **126**, 8648 (2004).
[28] Y. Suzuki, A. Takauchi, H. Takano, and H. Takenaka, Jpn. J. Appl. Phys. **1994**, 44 (2005).

[29]H. N. Chapman, A. Barty, S. Marchesini, A. Noy, S. P. Hau-Riege, C. Cui, M. R. Howells, R. Rosen, H. He, J. C. H. Spence, U. Weierstall, T. Beetz, C. Jacobsen, and D. Shapiro, J. Opt. Soc. Am. A **23**, 1179 (2006).

[30]Y. Takahashi, Y. Nishino, R. Tsutsumi, N. Zettsu, E. Matsubara, K. Yamauchi, and T. Ishikawa, Phys. Rev. B **82**, 214102 (2010).

[31]H. M. Quiney, A. G. Peele, Z. Cai, D. Patterson, and K. A. Nugent, Nat. Phys. **2**, 101 (2006).